# FENICS SIMULATION OF ARTESIAN CONDITIONS IN CLAY SLOPE

## K. Muratova[1], A. A. Abed[1], and M. Karstunen[1]

### KEYWORDS

Artesian conditions, Finite element method, FEniCS, safety calculation

### ABSTRACT

This paper presents a numerical simulation of the response of a slope with artesian conditions under the impact of a long heavy rainfall event. Sensitivity analysis of surface and bedrock inclination are presented. The robust FEniCS finite element tool is used to solve the governing coupled Hydro-Mechanical (HM) balance equations. An extended version of the Mohr-Coulomb model is implemented in Fortran and used as soil model. The paper discusses how the stability is influenced by changes in pore water pressure and the occurrence of artesian conditions, exploring slopes with different bedrock inclinations. It also presents potential failure surfaces as part of the discussion. The results provide better understanding of critical geological conditions, which helps to identify regions most at risk and take the required safety measures.

### 1. INTRODUCTION

In recent years, the world has witnessed a notable number of landslides, posing significant challenges to its infrastructure and communities. The understanding of triggering mechanism of landslides is crucial when aiming to predict and mitigate their occurrences.

Instability can happen even in almost horizontal landscapes. Even though most landslides are triggered by human activities, they can also have natural causes. The buildup of artesian pressure could be one of the reasons. Artesian conditions can be found in specific geological conditions: presence of both inclined bedrock beneath a clay deposit and layer of permeable soil between them resulting in a confined aquifer.

One of the most devastating landslides in Sweden, Tuve landslide in 1977, was initiated after a heavy rainfall event, involving artesian conditions [1]. The problem is expected to become even more severe with climate change and the

[1] Chalmers University of Technology , Gothenburg, Sweden, kseniia.muratova@chalmers.se

associated extreme weather conditions (i.e., more frequent heavy rainfall with long duration) which can lead to sudden pore water changes that can trigger landslides.

This paper aims to explore influence of artesian conditions on the slope stability. Three slope configurations with different inclinations of bedrock were chosen for investigation. For this purpose, Python code based on FEniCS finite element tool created by Abed et al. [2] was used. Additional functionalities have been added to the code to enable the modelling of artesian conditions, including the capability to model multiple soil layers.

## 2. METHOD

The code was utilised to solve the following balance equations:

### 1) Mechanical balance equations

$$\nabla \cdot \boldsymbol{\sigma} + \boldsymbol{b} = 0 \tag{1}$$

where $\nabla \cdot \boldsymbol{\sigma}$ is the divergence of the total stress tensor and **b** is a vector containing the body forces.

For considering unsaturated features of the problem, Bishop's effective stress is used:

$$\boldsymbol{\sigma}' = \boldsymbol{\sigma}'' + \chi \boldsymbol{s} \tag{2}$$

where $\boldsymbol{\sigma}'' = \boldsymbol{\sigma} - \boldsymbol{u_a}$ denotes the net stress, $\boldsymbol{s} = \boldsymbol{u_a} - \boldsymbol{u_w}$ is the matric suction. The pore air pressure and pore water pressure are denoted as $\boldsymbol{u_a}$ and $\boldsymbol{u_w}$, respectively. It is generally assumed that the pore air pressure remains at atmospheric levels with $u_a = 0$, so $\boldsymbol{s} = -\boldsymbol{u_w}$. Following the arguments by Gens et al. [3], the code assumes that $\chi = S_{eff}$ the effective degree of saturation, where:

$$S_{eff} = \frac{(S_r - S_{res})}{(S_{sat} - S_{res})} \tag{3}$$

with $S_r$ , $S_{sat}$ and $S_{res}$ refer to the soil degree of saturation at normal conditions, the degree of saturation at full saturation and the residual degree of saturation, respectively.

Additionally, information from the Soil Water Characteristic Curve (SWCC) is required to reflect the hydraulic properties of the unsaturated soil. In this study, the SWCC is assumed to have the following simple form (in fact is the code is flexible and any other formula can be easily implemented):

$$S_r = (S_{sat} - S_{res}) \cdot e^{-\alpha \cdot s} + S_{res} \tag{4}$$

where $\alpha$ is a material parameter. The corresponding hydraulic conductivity function is described by the equation:

$$K(s) = K_{sat} \cdot e^{-\alpha \cdot s} \tag{5}$$

The weak formulation of the mechanical balance equation and the finite element discretization yield:

$$\int_{\Omega} \nabla N_b^T \boldsymbol{M} \nabla N_b \delta \hat{u}\, d\Omega + \int_{\Omega} \chi \nabla N_b^T \boldsymbol{m^T} \nabla N_b\, \delta \widehat{u_w}\, d\Omega - \int_{\Omega} N_b\, \delta b d\Omega - \int_{\Gamma} N_b\, \delta \tau d\Gamma = 0 \tag{6}$$

where $N_b$ is a shape function, $\delta \hat{u}$ is the increment of nodal displacements, $\delta \hat{u_w}$ is the increment of nodal pore water pressure and $\delta\tau$ is the surface traction increment. The symbol $\boldsymbol{m^T}$ denotes the transpose of the unity vector and **M** represents the material stiffness matrix.

**Water mass balance equation**

The water mass balance equation for unsaturated soil can be written as (Abed and Sołowski [4]):

$$\nabla^T \left[ \frac{K(s)}{\rho_w g} \cdot (\nabla u_w + \rho_w g) \right] + n \left( \frac{\partial S_r}{\partial s} - \frac{S_r}{K_w} \right) \frac{\partial u_w}{\partial t} + S_r \frac{\partial \varepsilon_v}{\partial t} = 0 \tag{7}$$

where n is the porosity, $\rho_w$ is the density of water, $g$ is the gravity acceleration and $K_w$ is the water bulk modulus. To solve the equation both the SWCC and the hydraulic conductivity function are required to be defined. The term $\frac{\partial \varepsilon_v}{\partial t}$ is the rate of volumetric strain representing the coupling term with the mechanical behaviour.

The weak formulation of the water balance equation and the subsequent finite element discretization yield:

$$-\int_{\Omega} \nabla N_b^T \frac{K(s)}{\rho_w g} \nabla N_b\, \delta \widehat{u_w}\, d\Omega + \int_{\Omega} \nabla N_b^T \frac{K(s)}{\rho_w g} \rho_w g d\Omega + \int_{\Omega} \nabla N_b^T n \left( \frac{\partial S_r}{\partial s} - \frac{S_r}{K_w} \right) \frac{\partial \widehat{u_w}}{\partial t} d\Omega + \int_{\Omega} N_b\, S_r \frac{\partial \varepsilon_v}{\partial t} d\Omega = 0 \tag{8}$$

**Mohr-Coulomb (MC) model for unsaturated soil**

Using Bishop ‘s effective stress instead of Terzaghi’s effective stress, the standard form of MC model can be used directly:

$$f_M = \left(\frac{\sigma'_1 - \sigma'_3}{2}\right) - \left(\frac{\sigma'_1 + \sigma'_3}{2}\right) \cdot \sin\varphi' - c' \cdot \cos\varphi' \quad (9)$$

$$g_M = \left(\frac{\sigma'_1 - \sigma'_3}{2}\right) - \left(\frac{\sigma'_1 + \sigma'_3}{2}\right) \cdot \sin\psi \quad (10)$$

$$f_T = g_T = \sigma^t - \sigma'_3 \quad (11)$$

where $f_M$ and $g_M$ are the failure and the plastic potential surface, respectively, $fT$ is the tension cutoff failure surface, $\varphi$' is the effective internal friction angle, $c'$ is the cohesion intercept and $\psi$ is the dilatancy angle. Additionally, it is necessary to specify the tensile strength $\sigma^t$ , which is commonly defaulted to zero. Elasticity is governed by the classical Hooke's linear elasticity law, which relies on two material properties: the effective Young's modulus $E'$ and the effective Poisson's ratio $\upsilon'$.

## 3. ANALYSIS

During the analysis three models were created with different inclinations of frictional layers (i.e., indicated as 'permeable layer' in Figure 1). The models' geometries are presented in Figure 1. Identical volumes of infiltration of 0.45 $m^3$/day are applied to the top of all frictional layer to model environmental loads. The increased infiltration at the top boundary of the frictional layer is used to reflect the runoff due to the accumulation of water at the top of the surrounding, much less permeable, clay. Soil properties of clay, frictional layer and rock are summarised Table 1.

Table 1. Soil properties

| Property | Clay | Frictional layer | Rock | unit |
|---|---|---|---|---|
| MC properties | | | | |
| $\varphi'$ | 28 | 35 | 40 | [ º ] |
| c ′ | 3 | 20 | 20 | kN/$m^2$ |
| E | 3600 | 240000 | 1.0e7 | kN/$m^2$ |
| $K_{sat}$ | 1.16e-9 | 1.16e-5 | 1.16e-9 | m/s |
| Other properties | | | | |
| $\upsilon'$ = 0.2, $\psi$ = 0°, $\alpha$ = 0.01 1/kPa, $S_{sat}$ = 1, $S_{res}$ = 0.23, $K_0^{NC}$ = 0.6, $e_0$ = 0.667 | | | | |

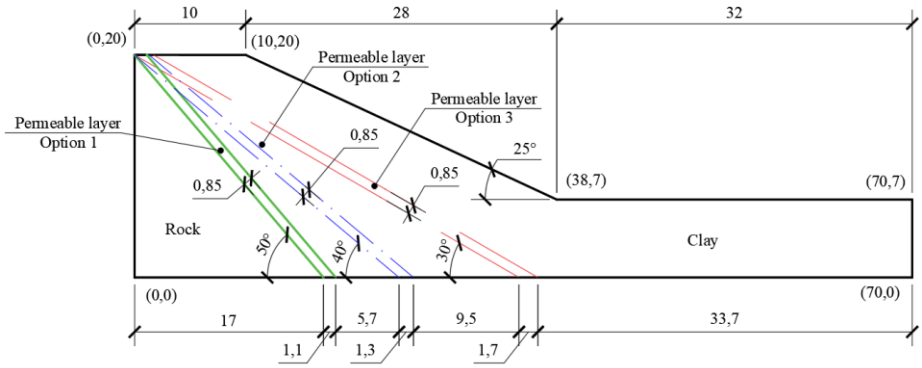


*Figure 1 Model geometry*

Firstly, the calculations of the stability of the slope in the initial conditions (water level at 0.5 meters above the bottom) using phi-c reduction (strength reduction) method were performed. The ratio between the available shear strength parameters to the critical ones needed to cause failure gives the safety factor SF:

$$SF = \frac{c'}{c'_{critical}} = \frac{\varphi'}{\varphi'_{critical}} \tag{7}$$

All three slopes in initial conditions have a safety factor higher than 1: 1.26, 1.40 and 1.69 that corresponds to frictional layer inclination of 50$^o$, 40$^o$ and 30$^o$, respectively.

Over time under environmental load, due to presence of the frictional layer between two impermeable layers, a confined aquifer is being formed. During this process the pore water pressures are increasing, displacements are developing, and stability is decreasing. The results of the analysis are presented in the following paragraphs.

**Displacements and failure**

Failures were observed after 14, 22, and 29 days of infiltration in cases 50, 40, and 30, respectively. Figures 2a-c show slip surfaces at the specified time (displacements are scaled by a factor of 100). White line depicts the contour of zero pore water pressure at failure. On the one hand, since case 50 has the smallest volume of the frictional layer, the rise of the water level happens faster, and it could be the reason of the faster failure. On the other hand, it also has the lowest initial safety factor which indicates that smaller changes in system can lead to failure. Additional investigation needed to understand which factors have the biggest impact.

Figure 3 illustrates horizontal surface displacement at points Q. An increase of the displacement rate is observed before failure. Since failure occurs relatively

fast, the pore water pressure in clay does not have enough time to dissipate and thus the deformation levels before failure are quite low. The largest surface displacements are noted in case 30, it is explained by the lowest thickness of the clay layer above the frictional layer and longest time until failure.

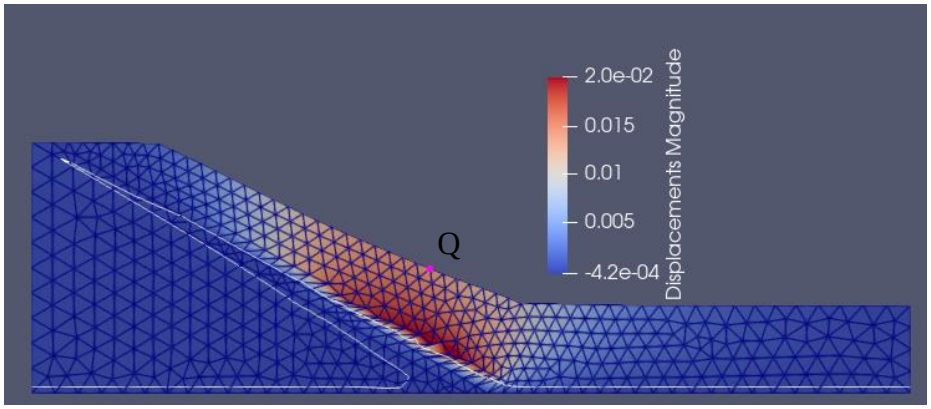


*Figure 2a. Displacements (in meters) of the model 30 at day 29*

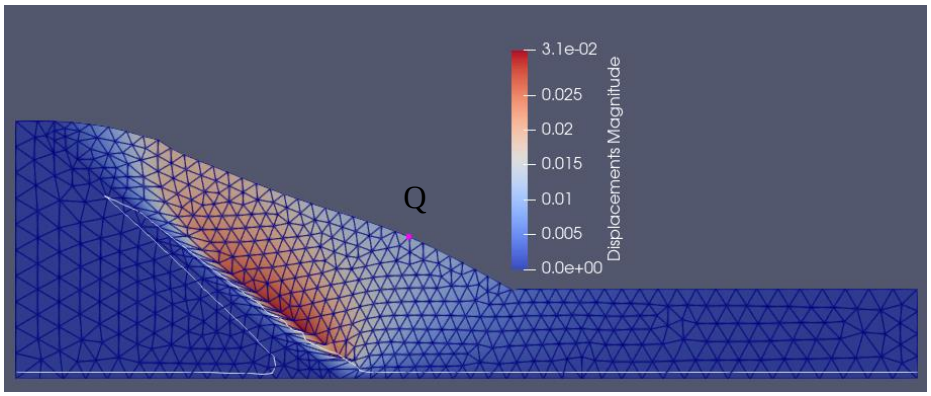


*Figure 2b. Displacements (in meters) of the model 40 at day 22*

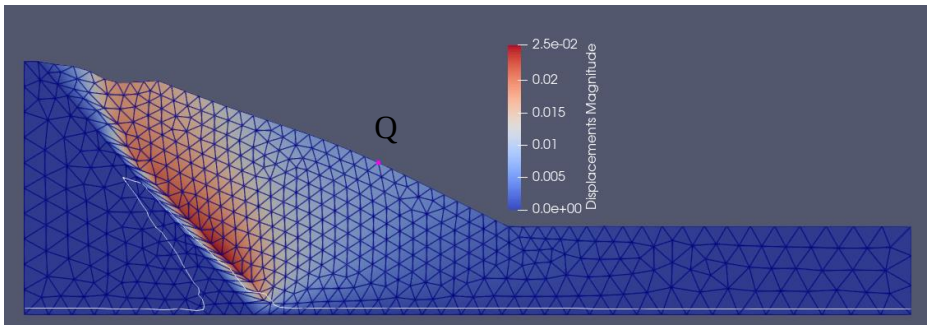


*Figure 2c. Displacements (in meters) of the model 50 at day 14*

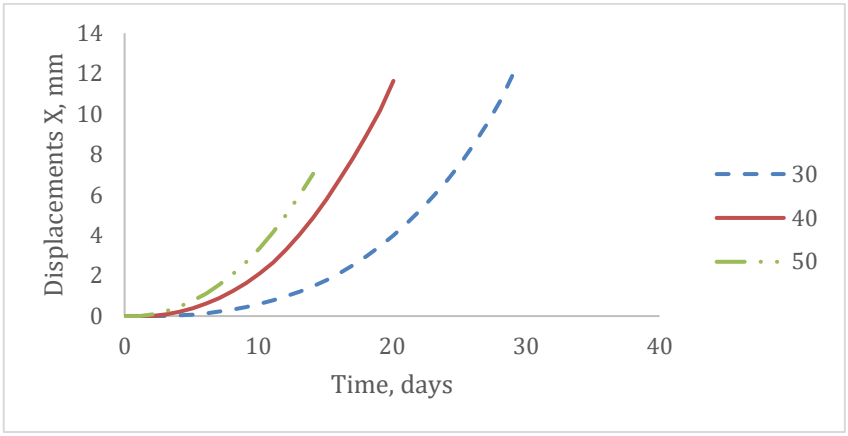


*Figure 3. Displacements at points Q over time until failure.*

**Pore water pressure**

Different distributions of suction along the layer due to different inclinations of frictional layers lead to different distribution of hydraulic conductivity over layer (see Figure 4), since the hydraulic conductivity is a suction dependant parameter, see Equation 5. The initial hydrostatic distribution of pore water pressure along the frictional layers of the three models is shown on Figure 5a. Due to the different variation of the hydraulic conductivity over depth and the different volume of the frictional layer with equal infiltration rate, the pore water pressure changes differently. The water level in the frictional layer in the case 30 increases slower than in case 50, case 40 showed intermediate result.

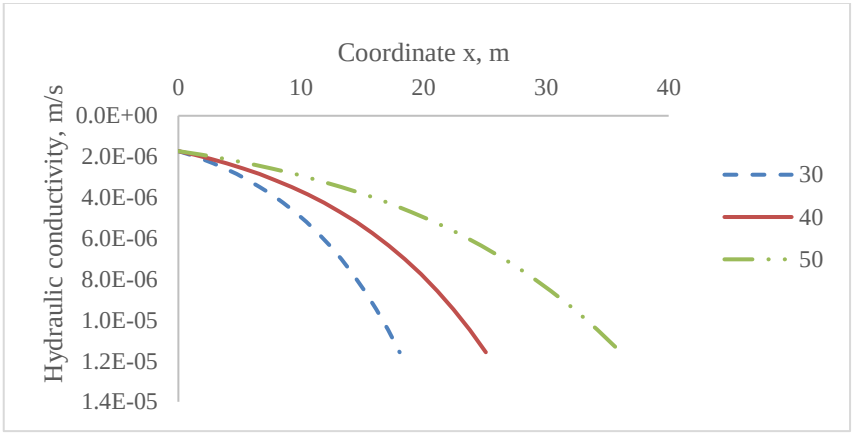


*Figure 4. Hydraulic conductivity along the frictional layer*

On Figure 5b-f the changes of pore water pressure over time are shown. At day 3, the water level in case A (50) has started to grow and pore water pressure started decreasing in contrast to case C (30) where pore water pressures stay constant. At day 10 in all cases the water level is increasing and the pore water

pressures at the bottom are decreasing. As seen in the figures, the minimum pore water pressures at bottom at failure are similar: -80 (Case 50), -88 (Case 40) and -85 (Case C), the different pressures are observed in the upper part of the slopes. The water levels at failures are at 12, 13 meters above bottom for cases 50 and 40 respectively. For case 30 frictional layer is almost fully filled with water – lowest point of the water level is at 14 meters above bottom, higest – at 18,7 meters.

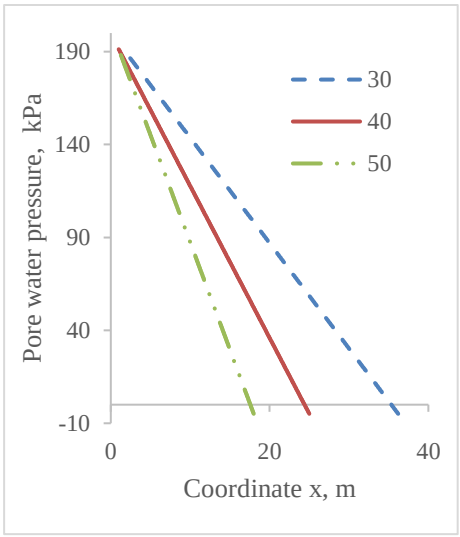


*Figure 5a. Initial pore water pressure along frictional layer*

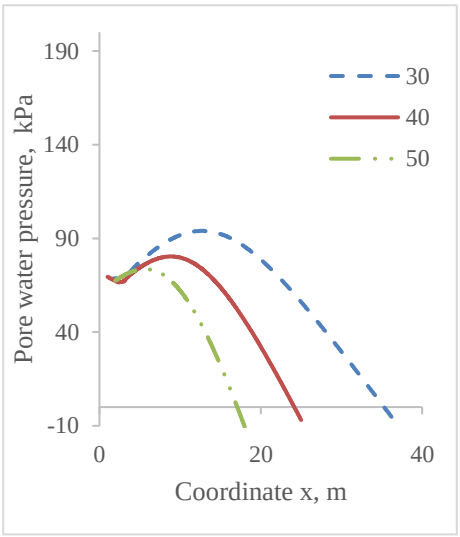


*Figure 5b. Pore water pressure along frictional layer at day 3*

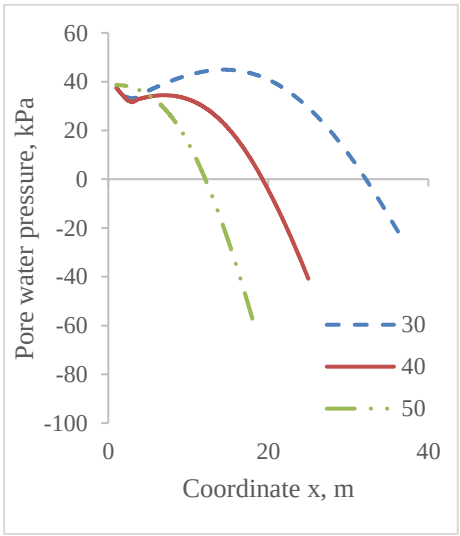


*Figure 5c. Pore water pressure along frictional layer at day 10*

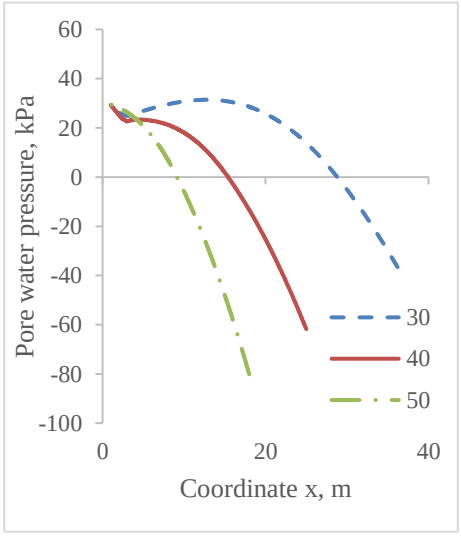


*Figure 5d. Pore water pressure along frictional layer at day 14*

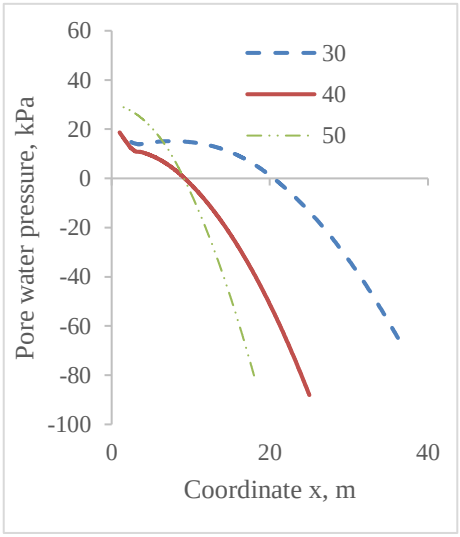


*Figure 5e. Pore water pressure along frictional layer at day 24*

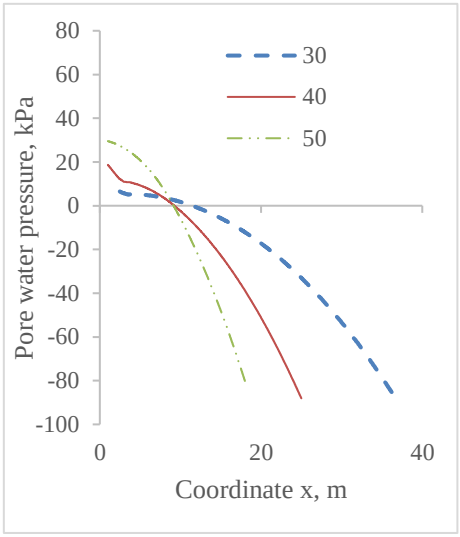


*Figure 5f. Pore water pressure along frictional layer at day 29*

## 4. CONCLUSIONS

Fully coupled hydro-mechanical analyses considering unsaturated conditions of the soils was performed to model the formation of artesian conditions due to environmental load. The effect of artesian conditions on slope stability was studied. The calculations showed that an infiltration of a specific duration and intensity leads to forming of artesian conditions when having specific geological conditions, which can trigger failure even in the case of relatively flat slopes. The main triggers of decreasing stability are 1) the increase of pore water pressure causing reduction in effective stress; 2) decrease of unsaturated part of the shear strength in the area where decrease of suction happens and 3) the specific stratigraphy of a thin frictional layer sandwiched between two impermeable layers leading to the development of artesian conditions after heavy rain event.

It must be emphasized that the use of this code, which uses many of the capabilities of the FEniCS platform, makes it possible to investigate complex time-dependant hydrogeological phenomena and opens opportunities to solve even more complex tasks. The capability of the code was even extended more by the new functionality of modelling layers with different soil properties which might look simple, but indeed it has far reaching consequences in increasing the flexibility of using FEniCS to model geotechnical problems. One example of these problems is the modelling of the development of artisan conditions as discussed in this paper. Since the problem is of interest and has a big impact on slope stability, further investigations are required to make more comprehensive conclusions.

## FUTURE RESEARCH

There are advancements of the code that needed to be implemented to model artesian conditions more realistically. Among the crucial ones is the implementation of different unsaturated behaviour of different layers. Different soil-water retention curves, such as van Genuchten are going to be implemented as well. In the future, different thermal and hydraulic boundary conditions will be inspected to analyse the slope stability under extreme environmental loads as driven by climate change. While the current work focuses so far on failure, the advanced material model Creep-SClay1S [5] that can consider important aspects of the clay behaviour such as anisotropy, rate-dependency and evolution of the fabric will be used to get more accurate predictions of the evolving pre-failure deformations.

## ACKNOWLEDGEMENT

The work is funded by Formas (Research Council for Sustainable Development, Grant (2021-02400) and the work is done as part of Digital Twin Cities Centre that is supported by Sweden's Innovation Agency VINNOVA (Grant 2019-00041).

## REFERENCES

[1] R. Larsson, M. Jansson: The Landslide at Tuve. Report No 18, Swedish Geotechnical Institute, 1982

[2] A. Abed, E. Gerolymatou, M. Karstunen: FEniCS simulation of a partially saturated slope under varying environmental loads. Proceedings 10th NUMGE, 2023.

[3] A. Gens, M. Sánchez, D. Sheng: On constitutive modelling of unsaturated soils. Acta Geotechnica 1, 137–137, 2006.

[4] A. Abed, W. Sołowski: A study on how to couple thermo-hydro-mechanical behaviour of unsaturated soils: Physical equations, numerical implementation and examples. Computational Geotechnics 92, 132–155, 2017.

[5] J.-P. Gras, N. Sivasithamparam, M. Karstunen, J. Dijkstra: Permissible range of model parameters for natural fine-grained materials. Acta Geotechnica, 13(2), 387–398, 2018.